Molecular Dynamics of Acetylcholinesterase Dimer Complexed with Tacrine

Stanislaw T. Wlodek,*,† Terry W. Clark,† L. Ridgway Scott,† and J. Andrew McCammon*,‡

Contribution from the Texas Center for Advanced Molecular Computation, University of Houston, Houston, Texas 77204-5502, and Department of Chemistry and Biochemistry and Department of Pharmacology, University of California at San Diego, La Jolla, California 92093-0365

Received April 17, 1997. Revised Manuscript Received July 7, 1997[⊗]

Abstract: We have studied the dynamic properties of acetylcholinesterase dimer from *Torpedo californica* liganded with tacrine (AChE−THA) in solution using molecular dynamics. The simulation reveals fluctuations in the width of the primary channel to the active site that are large enough to admit substrates. Alternative entries to the active site through the side walls of the gorge have been detected in a number of structures. This suggests that transport of solvent molecules participating in catalysis can occur across the porous wall, contributing to the efficiency of the enzyme.

Introduction

Acetylcholinesterase (AChE) catalyzes the hydrolysis of the neurotransmitter acetylcholine (ACh) at neuronal and neuromuscular synapses to yield choline and acetic acid.[1,2] AChE is known as one of the most kinetically efficient enzymes, operating at nearly the diffusion limit.[3,4] Several years ago, the crystal structure of the homodimeric AChE from *Torpedo californica* ray (TcAChE) was determined[5] followed by structures of its complexes with tacrine (THA), edrophonium, and decamethonium.[6] More recently, the structure of the mouse enzyme[7] and the *Torpedo californica* enzyme[8] complexes with the peptide fasciculin have been determined. Although analyses of the crystal structures have provided some essential insights into AChE activity, these insights have in turn raised new questions. For example, it is not clear how the ligands enter and leave the active site, which, in the crystal structures, appears to be accessible only by way of a long channel from the AChE surface. Indeed, this channel is itself too narrow at one point to allow entry of substrate ACh, so that structural fluctuations are required for the enzyme to operate.

Computational studies can aid in the interpretation of crystallographic, kinetic, and other experimental data on enzymes. Molecular dynamics (MD) studies of a fragment of TcAChE have pointed to a possible mechanism for the binding or release of ligand or solvent molecules, through a back door mechanism.[9] Subsequent experiments utilizing site directed mutagenesis provided no support for a kinetically essential back door,[10] but kinetic studies with fasciculin.[11,12] which appears to totally block the primary channel, [8,7] suggest the existence of other routes to the active site. Other simulations that used Brownian dynamics to study the kinetics of ligand binding to AChE indicate that the rate of the enzyme catalysis or inhibition can be increased by as much as two orders of magnitude by the steering of cationic ligands by the electrostatic field of the enzyme.[13−15] These simulations have all been based on the rigid crystallographic structure, leaving questions about how the large-scale fluctuations of the structure may influence the field and the intermolecular interactions of the enzyme.

In this report, we present the results from MD simulations of the complete AChE dimer complexed with THA in solution. These simulations are to our knowledge the first of the entire dimer. In this study, we investigate active-site accessibility and look for alternative routes connecting the active site with the protein surface. From the dimer data, we perform analyses designed to detect large-scale, concerted motions and possible effects of oligomerization on reactivity. We chose to simulate the cation liganded enzyme, rather than unliganded, based on previous results from our group suggesting that a monovalent cation is always bound in the active site of AChE.[16] The cation, so positioned, is thought to support AChE's catalytic machinery. In addition, THA is a reversible inhibitor of AChE, now used as a drug for the treatment of Alzheimer's disease, further motivating these studies.

† University of Houston.
‡ University of California at San Diego.
⊗ Abstract published in *Advance ACS Abstracts,* September 15, 1997.

(1) Barnard, E. A. Enzymatic destruction of acetylcholine. In *The peripheral Nervous System*, Hubbard, J. I., Ed.; Plenum Publishers: New York, 1974; pp 201−206.
(2) Taylor, P.; Radić, Z. *Ann. Rev. Pharm. Tox.* **1994**, *34*, 362−1642.
(3) Bazelyansky, M.; Robey, E.; Kirsch, J. F. *Biochemistry* **1986**, *25*, 125−130.
(4) Quinn, D. M. *Chem. Rev.* **1987**, *87*, 955−979.
(5) Sussman, J. L.; Harel, M.; Frolow, F.; Oefner, C.; Goldman, A.; Toker, L.; Silman, I. *Science* **1991**, *253*, 872−879.
(6) Harel, M.; Schalk, I.; Ehret-Sabatier, L.; Bouet, F.; Goeldner, M.; Hirth, C.; Axelsen, P.; Silman, I. *Proc. Natl. Acad. Sci. U.S.A.* **1993**, *90*, 9031−9035.
(7) Bourne, Y.; Taylor, P.; Marchot, P. *Cell* **1995**, *83*, 503−512.
(8) Harel, M.; Kleywegt, G.; Ravelli, R.; Silman, I.; Sussman, J. L. *Structure* **1995**, *3*, 1355−1366.
(9) Gilson, M. K.; Straatsma, T. P.; McCammon, J. A.; Ripoll, D. R.; Faerman, C. H.; Axelsen, P. H.; Silman, I.; Sussman, J. L. *Science* **1994**, *253*, 1276−1278.
(10) Kronman, C.; Ordentlich, A.; Barak, Dov; Velan, B.; Shafferman, A. *J. Biol. Chem.* **1994**, *269*, 27819−27822.
(11) Radić, Z.; Quinn, D. M.; Vellom, D. C.; Camp, S.; Taylor, P. *J. Biol. Chem* **1995**, *270*, 20391−20399.
(12) Rosenberry, T. L.; Rabl, C. R.; Neumann, E. *Biochemistry* **1996**, *35*, 685−690.
(13) Tan, R. C.; Truong, T. N.; McCammon, J. A.; Sussman, J. L. *Biochemistry* **1993**, *32*, 401−403.
(14) Antosiewicz, J.; McCammon, J. A.; Wlodek, S. T.; Gilson, M. K. *Biochemistry* **1995**, *34*, 4211−4219.
(15) Antosiewicz, J.; Wlodek, S. T.; McCammon, J. A. *Biopolymers* **1996**, *39*, 85−94.
(16) Wlodek, S. T.; Antosiewicz, J.; McCammon, A.; Gilson, M. K. Binding of cations and protons in the active site of acetylcholinesterase. In *Modelling of Biomolecular Structures and Mechanisms*; Pullman, A., Jortner, J., Pullman, B., Ed.; Kluwer Academic Publishers: 1995; pp 25−37.

S0002-7863(97)01226-2 CCC: $14.00

Methods

The MD simulations described below were performed with the program EULERGROMOS,[17] a parallel version of the well-known simulation program GROMOS.[18] EULERGROMOS assigns contiguous spatial elements (of the simulation box) to individual processes, whereby processes essentially perform molecular dynamics locally on their set of atoms, updating boundary data with other processes at regular intervals. The design of EULERGROMOS makes it well suited for distributed-memory, massively parallel computers such as the Intel Paragon; however, it can also run efficiently on shared-memory computers. Due to the aggressive spatial decomposition of the molecular system, EULERGROMOS can be used to simulate large protein systems in reasonable time. With periodic and selective outputting, the vast amount of generated trajectory data was reduced to manageable levels.[19]

Our simulation is based on the crystal structure of TcAChE liganded with the THA inhibitor.[6] Preparation of the initial system was recently described elsewhere.[20] Briefly, several missing residues from the original protein data bank file for the monomer were reconstructed with the aid of the molecular modeling software, InsightII.[21] The THA molecule, *ab initio* optimized with the 6-31G** basis set, was placed in the active site of the enzyme to fit with the crystal structure coordinates. The dimeric AChE−THA complex was then generated by rotating the monomer around the 2-fold crystallographic symmetry axis, after which the monomers were connected with the disulfide bond formed by the C-terminal Cys 537 residues. Protonated THA was represented by a GROMOS united atom model in consistency with the rest of the system, except the atomic charges which were assigned using the CHELPG procedure[22] with the 6-31G** wave function. The ionization state of the simulated protein was assigned by numerical titration of the monomeric AChE−THA complex for near-physiological conditions.[23] From the two lowest energy states, we used the titration state that firmly binds the THA ligand.[20] This configuration is characterized by neutral His 440, Glu 443, and Asp 392 residues; all other ionizable residues appeared to be in their standard protonation states, that is, all histidines neutral, with all acidic and basic residues ionized.

Further preparation included the addition of all missing polar hydrogen atoms in the AChE−THA dimer which we subsequently energy minimized with 200 steps of steepest descent. At this stage of system preparation a few residues were still involved in close interatomic contacts, so they were relaxed by energy minimization keeping all other residues fixed. Next, water molecules identified in the AChE−THA crystal structure were added since some may belong to the integral structure of the protein.[24] We hydrated the system with SPC/E water molecules in a rectangular box such that the minimum distance from the box walls to the protein atoms was not smaller than 1 nm and the minimum distance between water oxygen atoms and other heavy atoms was 0.25 nm. All water molecules were then energy minimized with steepest descent for 200 steps. Bulk water molecules that were found in protein cavities after minimization and that could not form at least two hydrogen bonds were removed; energy minimization of the remaining solvent molecules was repeated. The resulting system, huge by contemporary standards, contained 10 438 solute atoms and 39 863 water molecules in a $9.3 \times 9.7 \times 15.9$ nm^3 box.

We equilibrated the system beginning with dynamic equilibration of solvent molecules only (solute fixed) at 300 K for 20 ps with velocity reassignment from a Maxwellian distribution at 0.2 ps intervals. Equilibration of the solute was initiated with 200 steepest descent steps (solvent fixed), followed by dynamic equilibration of solute (solvent fixed) for 5 ps at 10, 50, 100, 200, and 298 K, with velocity reassignment at 0.2 ps intervals. Finally, dynamic equilibration of the entire system (solute and solvent) was performed at 298 K for 10 ps with 0.2 ps velocity reassignment. In all of this, energy minimization was performed with ARGOS[25] using GROMOS force field parameters; dynamic runs were performed with EULERGROMOS.

Following equilibration, a 500 ps MD simulation using an NTV ensemble was performed during which data were collected. The system was coupled to a temperature bath at 298 K with separate relaxation for solute and solvent using a relaxation time of 0.1 ps. We used a time step of 2 fs for the dynamics and a nonbonded-interaction cutoff radius of 1 nm; the trajectory was sampled every 0.04 ps (20 step intervals). Since outputting the entire system was prohibitive, we chose to reduce I/O costs and disk storage requirements by only outputting coordinates for the entire solute (10 438 atoms) and all crystal waters and bulk water located in the vicinity of the active site channels of each subunit.[19] Specifically, we monitored only those bulk water molecules which were within 18 Å from the O_η atom of Tyr 121 in the initial (equilibrated) structure. (The O_η atom of Tyr 121 is located approximately in the middle of reaction gorge.)

In this report, much of our analysis is in terms of the rms atomic deviations from the X-ray structure, $\mathrm{rmsd}_{\mathrm{X-ray}}$, and rms displacements from the cumulative average simulated structure, $\mathrm{rmsd}_{\mathrm{cum}}$. We compare the rms atomic fluctuations, $\langle \Delta \mathbf{r}_i^2 \rangle^{1/2}$, with the corresponding experimental values derived from the *B* factors

$$\langle \Delta \mathbf{r}_i^2 \rangle = 3B_i/(8\pi^2) \tag{1}$$

where $\boldsymbol{r}_i$ is a coordinate vector of atom i; we also compare the properties of the cumulative average structure with the crystal X-ray structure.

Global and intermonomer motion of the protein are determined by calculation of relative displacements of the monomer centers of mass (cm), of variation of relative orientation of reaction channel axes, and by diagonalization of the C_α displacement covariance matrix **C** which elements are

$$c_{ij} = \left(\frac{1}{M}\right)\sum_{k=1}^{M}\{x_i(k) - \langle x_i \rangle\}\{x_j(k) - \langle x_j \rangle\} \tag{2}$$

where M is the total number of configurations, and x_i are the

(17) Clark, T. W.; Hanxleden, R. V.; McCammon, J. A.; Scott, L. R. Parallelizing molecular dynamics using spatial decomposition. In *Scalable High Performance Computing Conference*; Knoxville, TN, 1994; pp 95−102. Available via anonymous ftp from softlib.rice.edu as pub/CRPC-TRs/reports/CRPC-TR93356-S.

(18) van Gunsteren, W. F.; Berendsen, H. J. C. *GROMOS: GROningen MOlecular Simulation sofware*; Laboratory of Physical Chemistry, University of Groningen; Nijenborgh, The Netherlands, 1988.

(19) Clark, T. W.; Scott, L. R.; Wlodek, S.; McCammon, J. A. I/O limitations in parallel molecular dynamics. In *Proceedings of the 1995 ACM/IEEE Supercomputing Conference*; Baker, F., Wehmer, J., Ed.; IEEE Computer Society Press: 1995. Available on CD-ROM and at http://www.supercomp.org/sc95/proceedings.

(20) Wlodek, S. T.; Antosiewicz, J; McCammon, J. A.; Straatsma, T. P.; Gilson, M. K.; Briggs, J. M.; Humblet, C.; Sussman, J. L. *Biopolymers* **1996**, *38*, 109−117.

(21) *InsightII*; Molecular Simulations, Inc.: San Diego, CA, 1996.

(22) Breneman, C. M.; Wiberg, K. B. *J. Comput. Chem.* **1990**, *11*, 361−373.

(23) Antosiewicz, J.; McCammon, J. A.; Gilson, M. K. *J. Mol. Biol.* **1994**, *238*, 415−436.

(24) Sreenivasan, U.; Axelsen, P. H. *Biochemistry* **1992**, *31*, 12785−12791.

(25) Straatsma, T. P.; McCammon, J. A. *J. Comput. Chem.* **1990**, *11*, 943−951.

Cartesian coordinates with overall translation and rotational motion removed. This matrix is especially useful for detecting the large-amplitude, essential motions of the macromolecule.[26−28] Columns of the matrix **V** which transforms **C** into a diagonal matrix Λ

$$\Lambda = \mathbf{V}^{\mathrm{T}}\mathbf{C}\mathbf{V} \tag{3}$$

are eigenvectors $\mathbf{v}_n$, belonging to the corresponding eigenvalues λ_n (the diagonal entries of Λ) and determine the direction of displacements of C_α atoms for each mode n.

We examined the active site geometry, particularly the active site entrance size, by generating the Connolly type probe-accessible surfaces[29] for both subunits of each trajectory sampled at 1 ps intervals, with a continuity search of those surfaces in the area of active site gorge.[9] One can estimate the entrance dimensions to the reaction channel for a given protein conformation by repeating the procedure with different probes of varying radii. We searched for alternative routes into the active site by constructing Lee and Richards solvent-accessible surfaces[30] generated with a 0.14 nm probe[9] using liganded and unliganded conformations with a 1 ps resolution.

Also, in view of the importance of the electric field in steering cationic ligands to the active sites, we examined fluctuations of the electric potential inside the reaction channel. The potential was obtained by solving the linearized Poisson−Boltzmann (PB) equation for selected dimer conformations with the use of the UHBD program.[31]

Results

Time Dependence of Selected Global Molecular Properties. In this section we provide evidence that our system preparation resulted in a properly equilibrated protein. Figure 1a shows that the total temperature (of about 296 K) and solute temperature (of about 284 K) are reasonably constant during the simulation. The slightly lower temperature of the solute is a common feature of simulations that use nonbonded cutoffs.[32] The total potential energy (Figure 1b) on the other hand levels off after the first 100 ps of the simulation. This initial drop can be attributed largely to solvent−solvent and solute−solvent interaction, because as Figure 1c shows the total nonbonded intrasolute potential energy is flat over the entire 500 ps. The decrease in the total potential energy in the first 100 ps reflects continued relaxation of the solvent, but it is of small magnitude, about 0.15 kJ/mol per atom, or about 6% of the mean kinetic energy per atom.

The rms deviations from the X-ray structure ($\mathrm{rmsd}_{\mathrm{X-ray}}$) of all heavy and backbone atoms versus simulation time are shown in Figure 2. The values were obtained by independent fits of each monomer to the crystal structure in order to eliminate the contribution of relative subunit motion. The continuous increase of the $\mathrm{rmsd}_{\mathrm{X-ray}}$ over the entire range of 500 ps indicates that the simulation is not converged within that time range, not surprising for a system of the size of AChE. Figure 2 also shows that starting from about 250 ps, the enzyme subunits begins to explore different regions of configuration space, but the difference in $\mathrm{rmsd}_{\mathrm{X-ray}}$ for subunits at 500 ps remains small, on the order of about 0.05 nm.

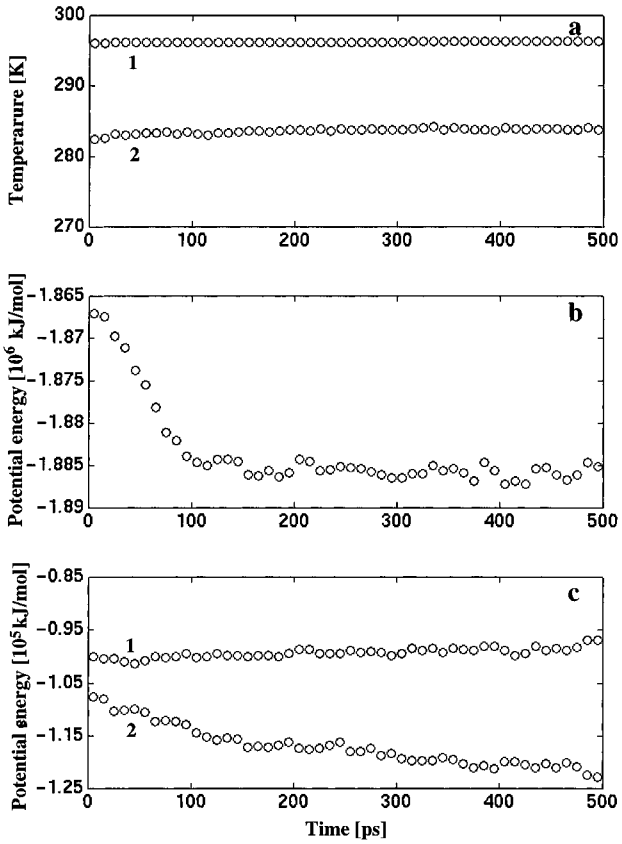

Figure 1. Variation of 10 ps averages of temperature and selected potential energies for the AChE−THA system in solution: (a) curve 1 is the total temperature, curve 2 is solute temperature; (b) total potential energy, and (c) curve 1 represents the total nonbonded intrasolute interactions, while curve 2 is the nonbonded potential energy for the solute−solvent interactions.

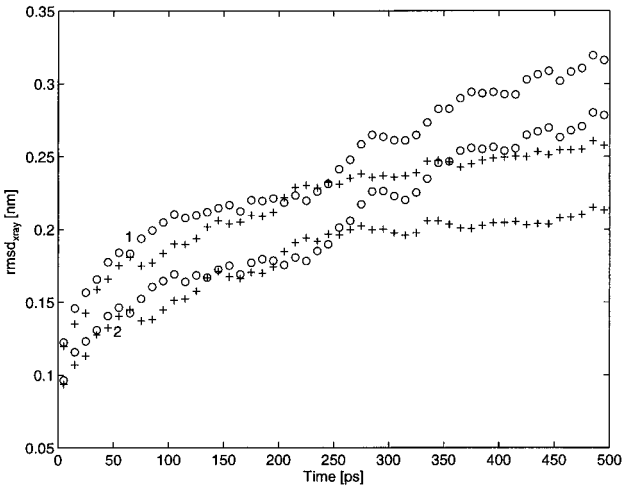

Figure 2. Time dependence of the rms deviation from the crystal structure ($rmsd_{\mathrm{X-ray}}$) for subunits A (circles) and B (crosses) of the AChE−THA complex, shown as 10 ps averages. Curves 1 refer to all heavy atoms deviations and curves 2 represent backbone atoms. In calculation of the $\mathrm{rmsd}_{\mathrm{X-ray}}$ shown on the figure, each monomer was separately fitted to the crystal structure.

Atomic Fluctuations and Properties of the Average Conformation. The time evolution of the rms fluctuation from the average structure, $\mathrm{rmsd}_{\mathrm{cum}}(t)$, provides a measure of the convergence of the dynamical properties of the protein. This function describing the fluctuations of all heavy atoms is plotted

(26) McCammon, J. A.; Harvey, S. C. *Dynamics of proteins and nucleic acids*; Cambridge University Press: Cambridge, UK, 1987.
(27) García, A. E. *Phys. Rev. Lett.* **1992**, *68*, 2696−2699.
(28) Amadei, A.; Linssen, B. M.; Berendsen, H. J. C. *Proteins* **1993**, *17*, 412−425.
(29) Connolly, M. L. *Science* **1983**, *221*, 709−713.
(30) Lee, B.; Richards, F. M. *J. Mol. Biol.* **1971**, *55*, 379−400.
(31) Davis, M. E.; Madura, J. D.; Luty, B. A.; McCammon, J. A. *Comput. Phys. Commun.* **1991**, *62*, 187−197.
(32) Wong, C. F.; Zheng, C.; Shen, J.; McCammon, J. A.; Wolynes, P. G. *J. Phys. Chem.* **1993**, *97*, 3100−3110.

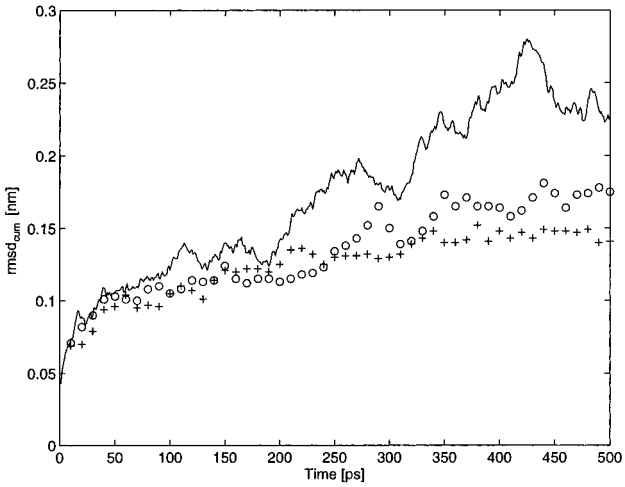

Figure 3. Time dependence of the all-atom rms displacement, $\mathrm{rmsd}_{cum}(t)$, of the AChE−THA dimer complex from the cumulative average structure derived from the simulation time interval $(0,t)$ (solid line), and for monomer A (circles) and B (crosses).

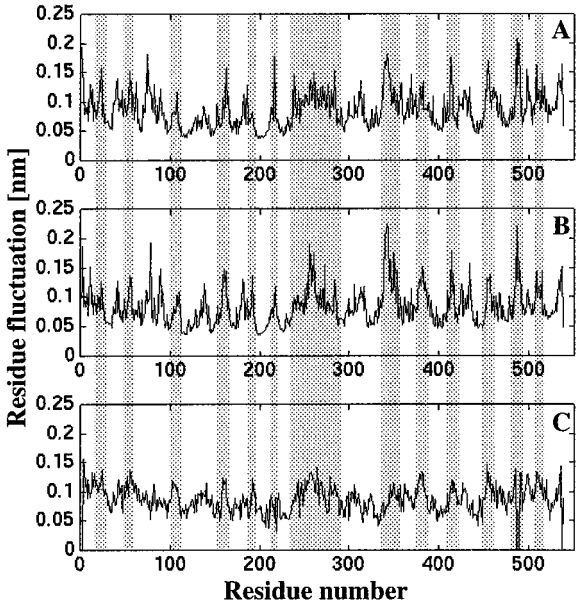

Figure 4. Residue fluctuations for subunits A and B of the AChE−THA complex obtained by averaging atomic fluctuations $\langle \Delta \mathbf{r}_i^2 \rangle^{1/2}$ derived from the 400−500 ps fragment of trajectory. Part C shows the respective experimental X-ray values (eq 1). Shaded areas highlight some of the regions of the protein with larger than average mobility in both the crystallographic and simulation analyses. Note that residues with fluctuations of zero in part C are in fact highly mobile; these residues were not localized in the crystal.

for the entire dimer and both subunits separately (Figure 3). The rms fluctuations of the heavy atoms in both subunits are reasonably similar and appear to converge to a value of 0.15−0.18 nm after about 300 ps. The contribution of the intermonomer motions is well visible on Figure 3 starting from about 200 ps. Figure 4 shows the atomic fluctuations averaged over residues for both AChE−THA subunits derived over the 400−500 ps time subrange. For comparison, the corresponding values obtained from the experimental *B* factors are also included. Figure 4 reveals a reasonably good agreement between calculated residue fluctuations in solution and the values obtained from the X-ray experiments.[6] The shaded areas in Figure 4 cover some of those regions of the protein which display enhanced mobility in the simulation and crystallographic analyses. All of those regions belong to the solvent exposed

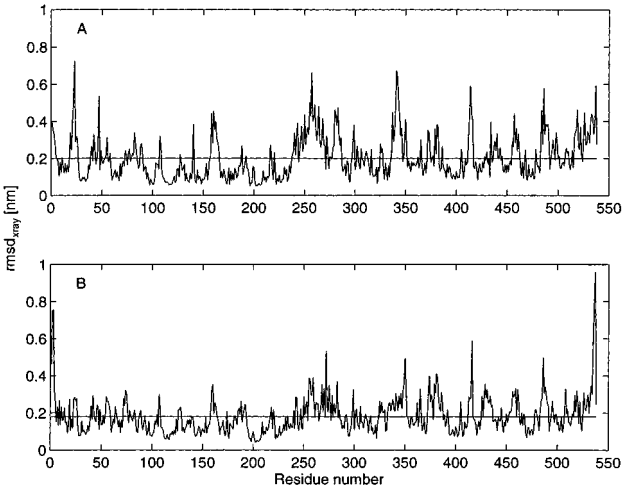

Figure 5. Root mean square deviations for each residue from the X-ray structure averaged over the 500 ps MD simulation. A and B refer to the two subunits of the enzyme. The horizontal lines mark the average value for all residues, which is 0.20 nm for monomer A and 0.18 nm for monomer B.

Table 1. rms Residue Fluctuations Derived from Last 100 ps of MD Simulation, $\langle \Delta \mathbf{r}^2 \rangle_{sim}^{1/2}$, and from Experimental *B* Factors, $\langle \Delta \mathbf{r}^2 \rangle_{exper}^{1/2}$ (in nm), and Average rms Deviations (rmsd_{X-ray}) from the X-ray Structure (in nm) Obtained from the Entire 500 ps Simulation for Selected Key Residues of Both Subunits[a]

			A		B	
function	residues	$\langle \Delta \mathbf{r}^2 \rangle_{exper}^{1/2}$	$\langle \Delta \mathbf{r}^2 \rangle_{sim}^{1/2}$	rmsd_{X-ray}	$\langle \Delta r^2 \rangle_{sim}^{1/2}$	rmsd_{X-ray}
I	Trp 84	0.07	0.07	0.23	0.05	0.15
	Glu 199	0.07	0.04	0.16	0.04	0.08
	Phe 330	0.06	0.09	0.17	0.08	0.22
II	Gly 118	0.06	0.04	0.06	0.04	0.09
	Gly 119	0.05	0.05	0.06	0.04	0.08
	Ala 201	0.07	0.04	0.07	0.04	0.07
III	Ser 200	0.07	0.04	0.15	0.04	0.10
	Glu 327	0.08	0.06	0.25	0.05	0.26
	His 440	0.06	0.05	0.33	0.05	0.16
IV	Trp 233	0.05	0.06	0.08	0.06	0.11
	Phe 288	0.09	0.07	0.13	0.05	0.12
	Phe 290	0.06	0.06	0.17	0.06	0.12
	Phe 331	0.06	0.06	0.13	0.05	0.10
	THA	0.09	0.06	0.28	0.05	0.25

[a] Residues in this table are components of quaternary ammonium binding locus (I), oxyanion hole (II), catalytic triad (III), and acyl binding pocket (IV). Data for THA are also included.

areas of the enzyme. As might be expected, a similar pattern is found for the average deviations of residues from their crystal structure positions (Figure 5). Figure 6 displays elements of the average structure and fluctuations and compares these with the X-ray data.

Fluctuations and rmsd_{X-ray} values for key residues essential for the AChE catalytic action and binding of THA inhibitor are presented in Table 1. Those data show that the catalytic residues as well as the THA molecule belong to relatively stable parts of the system. A few functional residues, Trp 84, Glu 327, His 440 in monomer A, Phe 330, and Glu 327 in monomer B, have somewhat larger rmsd_{X-ray} than the average value of 0.20 and 0.18 nm for monomers A and B, respectively. The modest displacements of those residues in the average structure relative to the X-ray structure are illustrated in Figure 6c for each subunit. Throughout the simulation, the tacrine molecule is directly hydrogen bonded to the oxygen atom of His 440 in monomer A through its ring nitrogen atom; in monomer B the direct hydrogen bond is replaced at about 50 ps (data not shown) by a solvent-mediated hydrogen bond. The second polar group

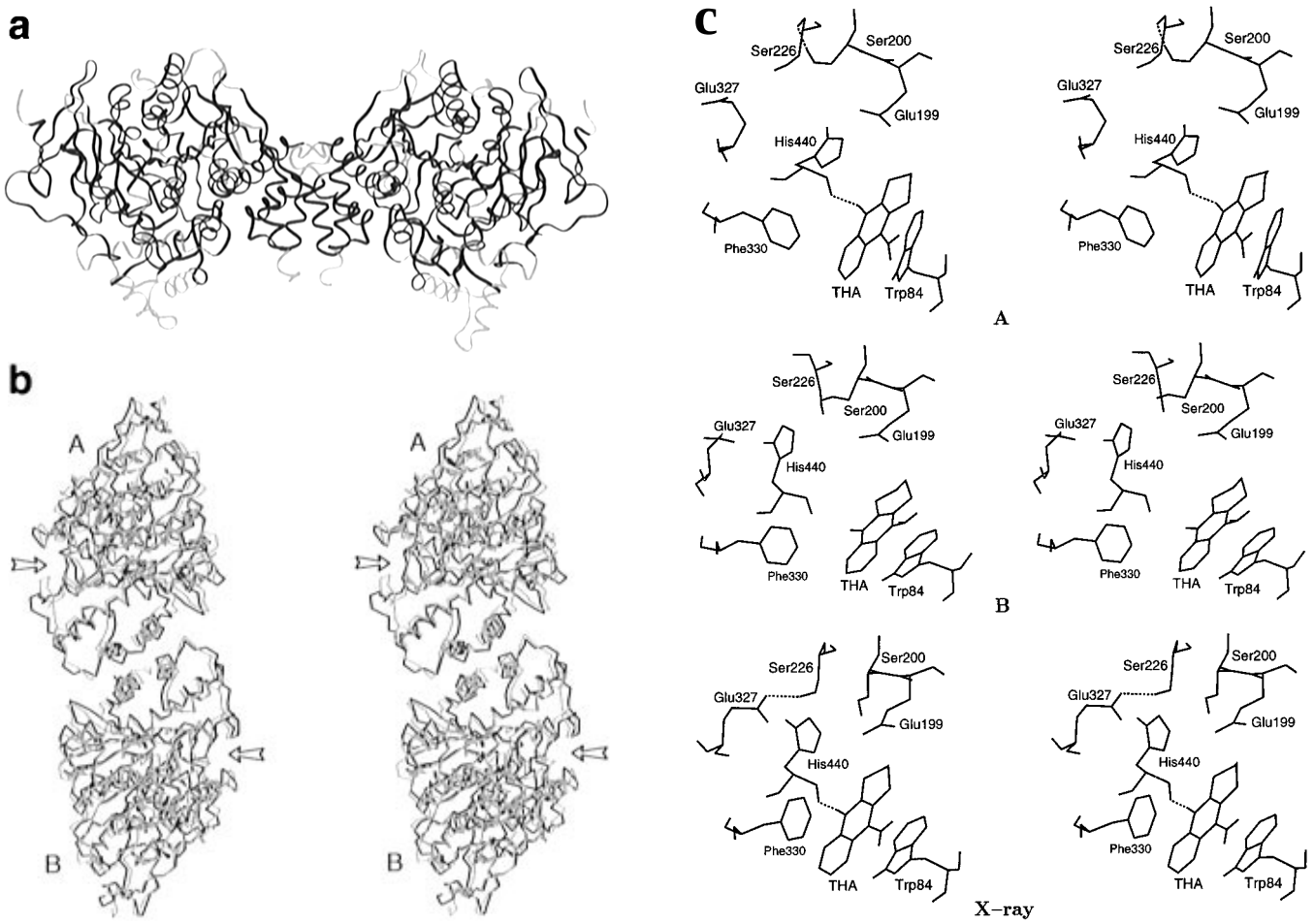

Figure 6. (a) Ribbon image of the average structure of the ACHE−THA complex. Grey fragments display higher than average mobility. (b) Stereo C_α traces of superimposed cumulative average structure (black solid lines) onto X-ray structure (light lines). Arrows indicate entrances to active site gorges. (c) Stereo images of the active site area in monomer A and B of the cumulative average structure and in X-ray structure. Broken lines indicate hydrogen bonds.

of THA (amino group) remains hydrogen bonded to solvent molecules, which undergo exchanges with other crystal and bulk water molecules. In both cases, however, the THA inhibitor remains in a stable position stacked above the indole plane of the Trp 84 residue.

In Table 2 we present fluctuation and $rmsd_{X-ray}$ data for all secondary structure elements of AChE. We again see that protein fragments such as α helix 5, 6, and 7, in monomer A, helix 6 in monomer B, and β strand 14 in both subunits undergo larger than average fluctuations largely due to their exposure to solvent. A component of the intermonomer bundle, helix 15, also shows larger than average $rmsd_{X-ray}$ value.

The (Cys 67-Cys 94) loop containing the Trp 84 residue (belonging to the helix h1) is largely responsible for the binding of cationic ligands, including ACh.[33,6,34] Furthermore, studies suggest that the large motion of this loop controls the binding activity of Trp 84 by selecting active or nonactive conformations via blocking the access of substrates.[35,36] In our simulation, the fluctuations of this loop are not large (last row, Table 2), although a similar loop undergoes extensive motion in related lipases.[37−39] This lack of unusual motion might indicate a difference between AChE and the lipases. However it might also be the result of limited simulation time or of the interaction between the THA and the indole ring of Trp 84, which could play a role in limiting the mobility of the loop.

Intermonomer and Global Motion. Figure 7 shows distance between the cm's of the monomers as a function of time and the relative orientation of the two reaction gorges measured as a dihedral angle between their axes. We see that AChE contracts slightly within the 100−500 ps time range with a simultaneous small rotation of subunits relative to each other. The time courses shown in Figure 7 suggest that both motions belong to low frequency global modes, with possibly a contribution from the relaxation of the protein from its initial state. The essential motion analysis based on diagonalization of the covariance matrix (eq 2) also reveals the existence of such global motions in our 0.5 ns simulation. Figure 8 shows projections

$$p_n(t) = \mathbf{v}_n \cdot \mathbf{r}_\alpha(t) \qquad (4)$$

of the C_α trajectory, $\mathbf{r}_\alpha(t)$, on the first five eigenvectors $\mathbf{v}_n$ of

(33) Ordentlich, A.; Barak, D.; Kronman, C.; Flashner, Y.; Leitner, M.; Segall, Y.; Ariel, N.; Cohen, S.; Belan, B.; Shafferman, A. *J. Biol. Chem.* **1993**, *268*, 17083−17095.

(34) Harel, M.; Quinn, D. M.; Nair, H. K.; Silman, I.; Sussman, J. L. *J. Am. Chem. Soc.* **1996**, *118*, 2340−2346.

(35) Ordentlich, A.; Barak, D.; Kronman, C.; Ariel, N.; Segall, Y.; Velan, B.; Shafferman, A. *J. Biol. Chem.* **1995**, *270*, 2882−2091.

(36) Barak, D.; Ordentlich, A.; Bromberg, A.; Kronman, C.; Marcus, D.; Lazar, A.; Ariel, N.; Velan, B.; Shafferman, A. *Biochemistry* **1995**, *34*, 15444−15452.

(37) Grochulski, P.; Li, Y.; Schrag, J. D.; Cygler, M. *Protein Sci.* **1994**, *3*, 82−91.

(38) Derewenda, U.; Swenson, L.; Wei, Y.; Green, R.; Kobos, P. M.; Joerger, R.; Haas, M. J.; Derewenda, Z. S. *J. Lipid Res.* **1994**, *35*, 524−534.

(39) Peters, G. H.; Olsen, O. H.; Svendsen, A.; Wade, R. C. *Biophys. J.* **1996**, *71*, 119−129.

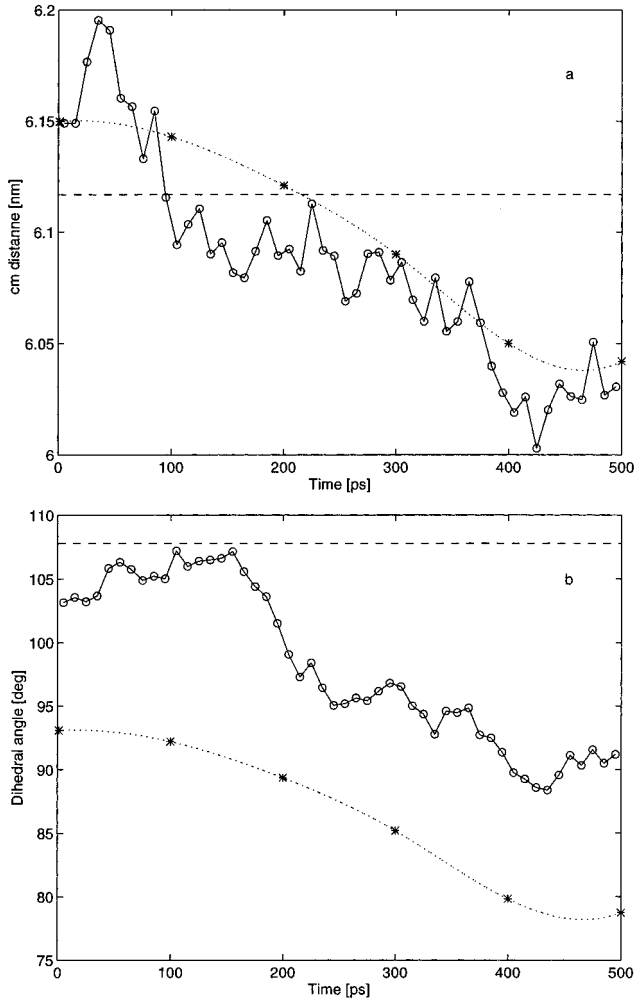

Figure 7. Time dependence of (a) the distance between the monomer centers of mass (cm) and (b) the dihedral angle between the reaction gorge axes shown as 10 ps averages (circles). The axis of a gorge was taken as a line connecting the C_δ of Ile 444 and a geometrical center of four atoms: C_α of Glu 73, C_β of Asn 280, C_γ of Asp 285 and O of Leu 333. Broken lines are set at the values for the X-ray structure. Stars show the similar dependences for C_α traces projected on the first eigenvector of covariance matrix, while dotted lines are cubic spline fits to the corresponding distance/angle values. Note that the cm and gorge directions in projected structures have to be defined with the C_α atoms only, resulting in a visible "phase shift" for the dihedral angle dependence.

the covariance matrix for the entire AChE dimer, ordered by the size of the corresponding eigenvalues. From the probability distribution for the displacements along corresponding eigenvectors (Figure 8, right side) it is clear that at least the first four modes are far from a Gaussian distribution. The first mode, responsible for about 66.5% of the overall motion, is likely to be a conformational transition which begins at about 150 ps, persisting until about 420 ps. The time dependence shown in Figure 7 has a similar pattern suggesting that the conformational change described by mode number 1 includes the overall movement of the subunits with respect to each other. The time variation of the cm distance and of the dihedral angle between the gorge axes in the overall motion can be compared to the corresponding variations in structures

$$\mathbf{r}_\alpha^m(t) = \mathbf{V}^{-1}\mathbf{p}^m(t) \tag{5}$$

projected on the the first eigenvector ($m = 1$) where, in the

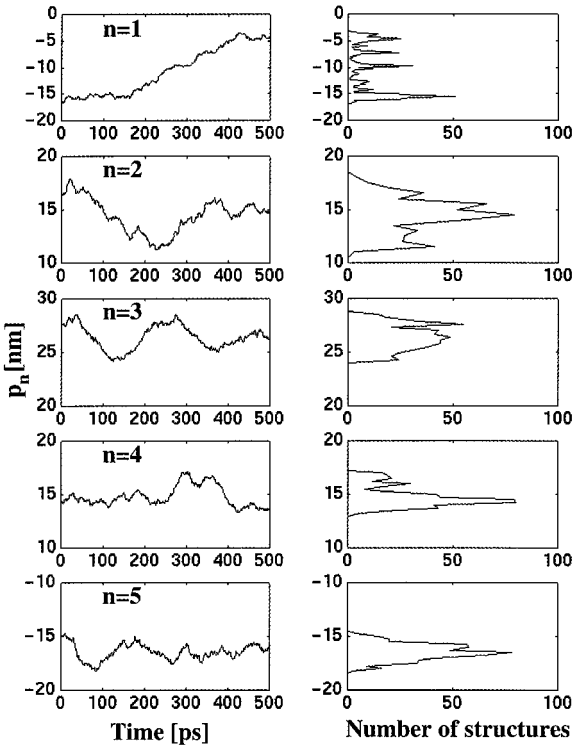

Figure 8. Time courses of the C_α trajectory projections, p_n, along the first five eigenvectors of its covariance matrix. Right side histograms show the corresponding probability distributions. The contributions of first five modes to the overall motion of C_α carbons calculated as fractions of the corresponding eigenvalues, $\lambda_i/\sum_i\lambda_i$ are 66.5, 8.7, 4.2, 3.1, and 1.8%, respectively.

projection vector $\boldsymbol{p}^m(t)$ defined as

$$\mathbf{p}^m(t) = [p_1(0), p_2(0), ..., p_{m-1}(0), p_m(t), p_{m+1}(0), ..., p_{3N}(0)]^T \tag{6}$$

all components except that for the mode m are set at values for time $t = 0$. In fact, Figure 7 shows that the character of those two time dependences match each other well, confirming our suggestion that the first dominant mode describes most of the intermonomer motion.

Accessibility of the Active Site. Soon after the solution of the AChE crystal structure revealed that the catalytic machinery of the enzyme is located at the bottom of the long and narrow gorge,[5] the mechanism of the fast binding of substrate and inhibitors became a key area of interest. The electric field inside the channel plays an important role in rate acceleration of the diffusional encounter between the charged substrate and the AChE active site area permitting substrate hydrolysis at nearly the collision rate.[14,15] The simplest kinetic mechanism assumes that the reaction channel is open large enough to allow a substrate of acetylcholine's size to reach the bottom. In the current MD simulation we estimated the size of the channel opening in structures sampled at 1 ps intervals using a Connolly-type probe-accessible surface. Figure 9 shows the fluctuations of the opening measured as the maximum radius (from a set of 0.12, 0.14, 0.16, 0.18, 0.20, 0.22, 0.24, and 0.26 nm) of a probe for which the molecular surface is continuous from the entrance to the bottom of the gorge area. The corresponding distributions of opening size are shown in Figure 10. It is seen that AChE−THA fluctuates rapidly between closed and open structures up to about 0.52 nm in diameter, adequately sized to admit substrate. In Figure 11 examples of two extreme cases are shown as 0.14 nm probe-accessible surfaces. For comparison, a corre-

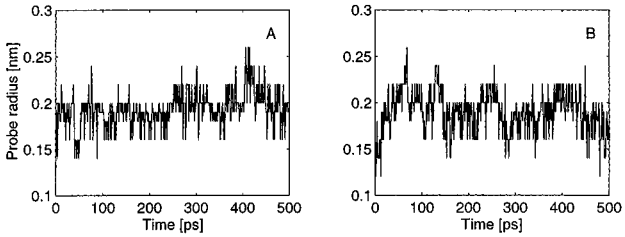

Figure 9. Fluctuation of gorge size in A and B subunits of the AChE−THA complex measured as the maximum radius of a probe used for generation of a continuous probe-accessible surface in the reaction gorge area. Sampling for gorge size opening was every 1 ps.

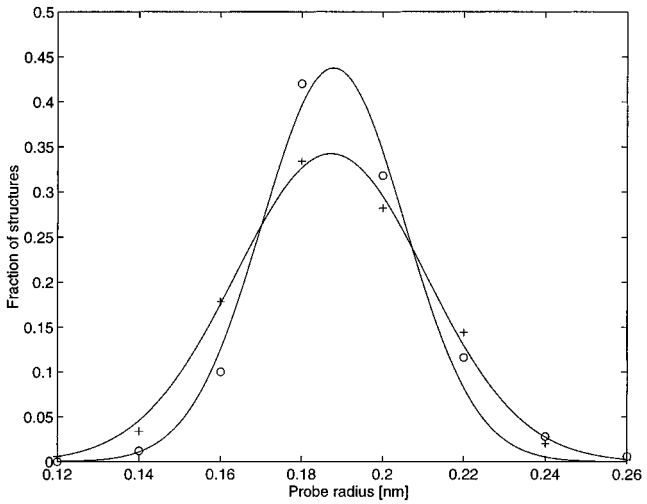

Figure 10. Distribution of gorge opening sizes from Figure 9. Circles and crosses are for subunits A and B, respectively. Solid lines are best Gaussian fits to the simulated values.

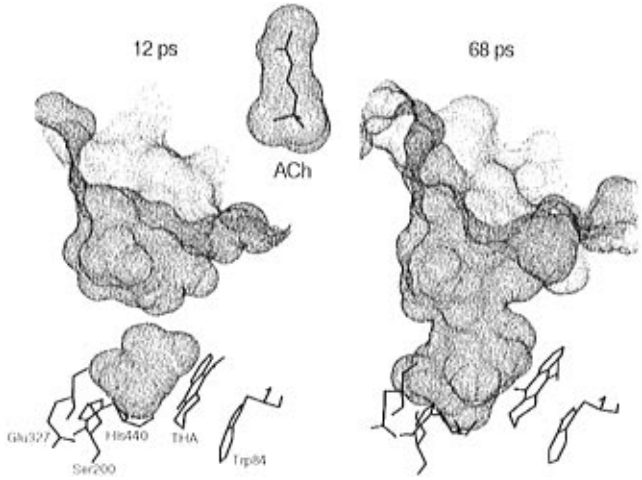

Figure 11. Fragments of solvent-accessible surfaces from the reaction gorge area in subunit B generated for snapshots at indicated simulated times, illustrating extreme cases of fully closed and fully open gorge. A solvent-accessible surface of the substrate ACh is shown for comparison.

sponding surface of ACh substrate is also included. The time scale and the range of the measured fluctuations in our simulations suggest that AChE is capable of accepting substrate without significant delay;[40,41] particularly given the favorable electric field inside the gorge,[14] the location of catalytic residues does not seem to impose a significant limitation on the binding rate.

(40) McCammon, J. A.; Northrup, S. H. *Nature* **1981**, *293*, 316−317.
(41) Szabo, A.; Shoup, D.; Northrup, S. H.; McCammon, J. A. *J. Chem. Phys.* **1982**, *77*, 4484−4493.

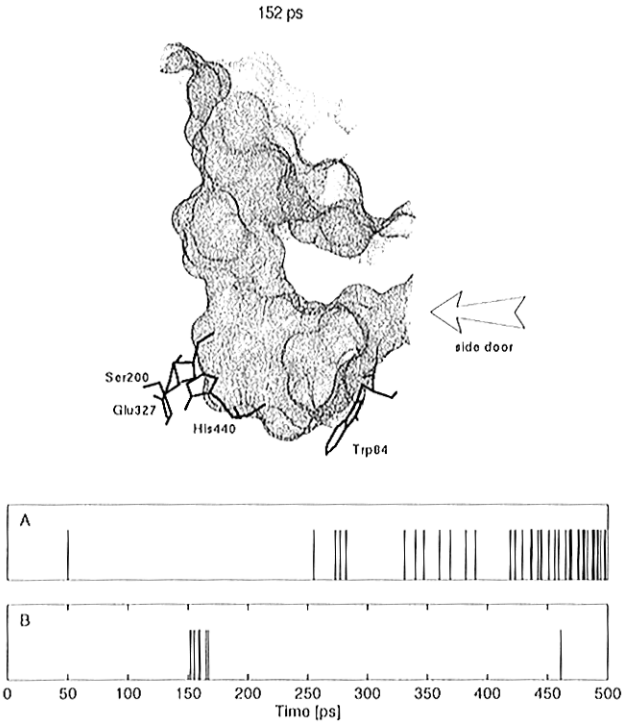

Figure 12. Fragment of the solvent-accessible surface for subunit B in a snapshot displaying an open side door after removal of THA inhibitor from the active site. Diagram at the bottom shows the trajectory structures in each subunit where any side openings occur. Frequency of sampling was every 1 ps.

In the current simulation we did not detect any back door opening as observed in the simulation of an unliganded AChE monomer.[9] A possible reason for that is the presence of the THA inhibitor during the current simulation. We did, however, observe a number of structures with side channels connecting the gorge with the protein surface when the THA molecule was removed from the active site. An example of such a "side door" is illustrated on Figure 12 along with a diagram showing the frequency of such openings. The opening through the side wall of the reaction gorge shown on Figure 12 is relatively large: it allows a probe of up to about 0.175 nm in radius to penetrate into or out of the reactive site. In fact, two bulk solvent molecules which at 0 ps were located outside the wall have penetrated inside the side channel shown on Figure 12, while two others have migrated close to its mouth. This opening was observed in subunit B starting at about 152 ps and lasted for about 19 ps (see the lower diagram on Figure 12); however, similarly to the main channel, its size has fluctuated ranging from completely closed (<0.14 nm) to about 0.175 nm. The image on Figure 13b shows that this opening is formed by the displacement of Glu 82, Pro 76, and Gly 77 with some smaller contribution from the movement of Asp 72, Glu 73, and Asn 85. One of the bulk water molecules which penetrated inside this channel formed hydrogen bonds with NH groups of Gln74 and Phe75 and with the main chain oxygen of Asp72. The opening observed in the same subunit at 461 ps allows probes barely larger than 0.14 nm in radius and is formed by nearly 90° rotation of the phenyl ring in Phe 78 and the displacement of Val 431 and Trp 432. The latter moves away from Gly 80, and in effect a narrow bent channel is formed. The side doors in subunit A were observed much more frequently (the upper diagram on Figure 12), but their size was usually close to 0.14 nm. It is interesting that the opening observed at about 50 ps contains two closely located channels shown on Figure 13a: The left side aperture is similar to that formed in subunit B at

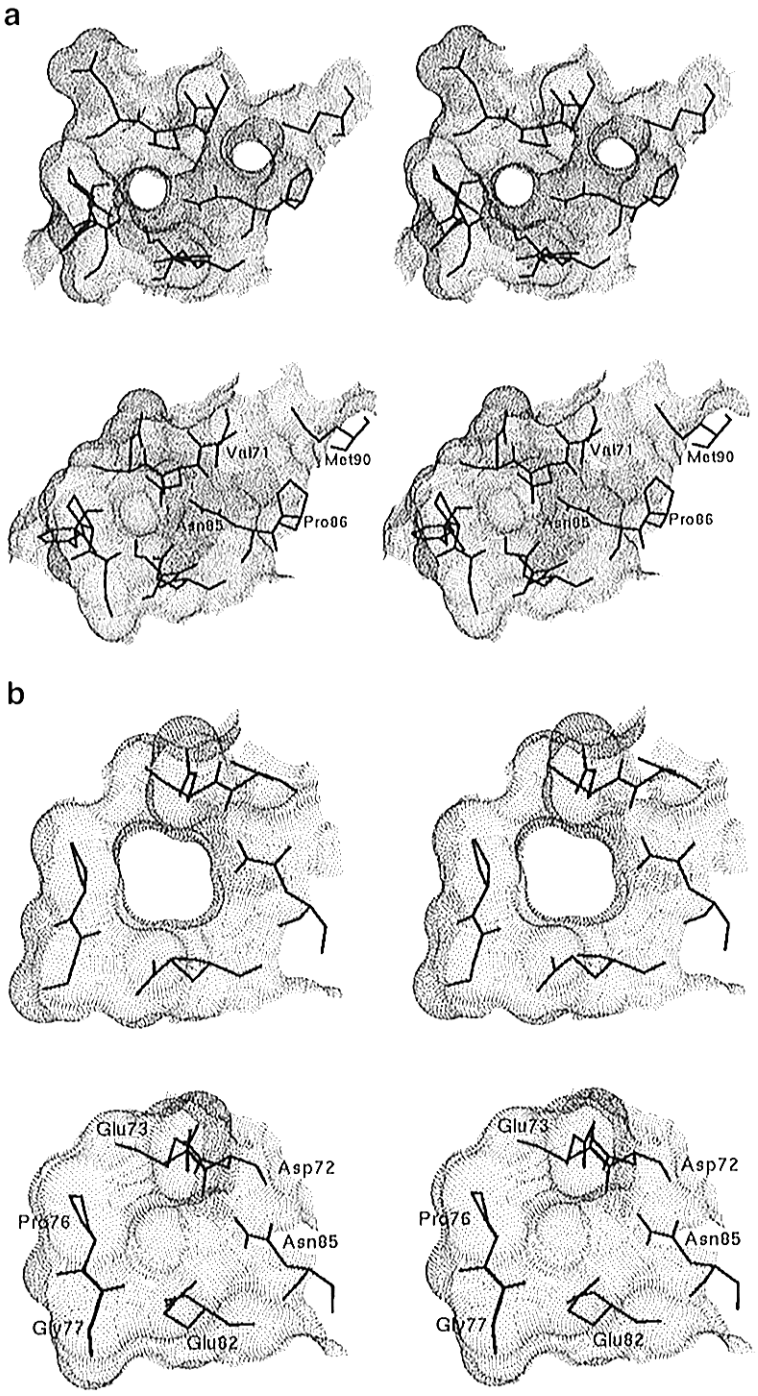

Figure 13. Examples of the openings in the wall of the gorge formed by the (Cys 67-Cys 94). (a) Stereo image of a relevant fragment of monomer A at 50 ps (upper image) (b) similar image for monomer B at 152 ps (upper image). Lower images show the corresponding fragments of solvent-accessible surface in the X-ray structure.

152 ps, while the second arises between Val 71, Asn 85, Pro 86, and Met 90. The single opening formed at 273 ps in this monomer is due nearly entirely to the movement of Trp 432 approximately in the plane of its indole ring as shown on the Scheme 1.

It emerges between Phe 75, Phe 78, Ile 333, and Pro 433. Another type of opening in subunit A is formed for simulation times approaching 500 ps. For example, at 488 ps the alterative channel which starts at about Trp 84 parallel to its indole ring passes close to the phenyl ring of Phe 78 and along main chain of Gly 80 and Ser 81 and is separated from the main gorge by Tyr 334. It emerges in proximity to the primary channel entrance between Phe 75 and Gln 74 side groups. It is interesting that whatever the topology of alternative route to the active site is, the motion of residues from the (Cys 67-Cys 94) loop participate largely in its formation.

Scheme 1

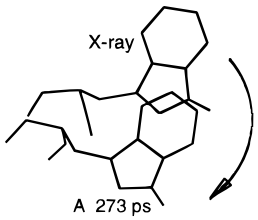

The formation of the side entries and the observed solvent penetration into one of them suggests that those openings might

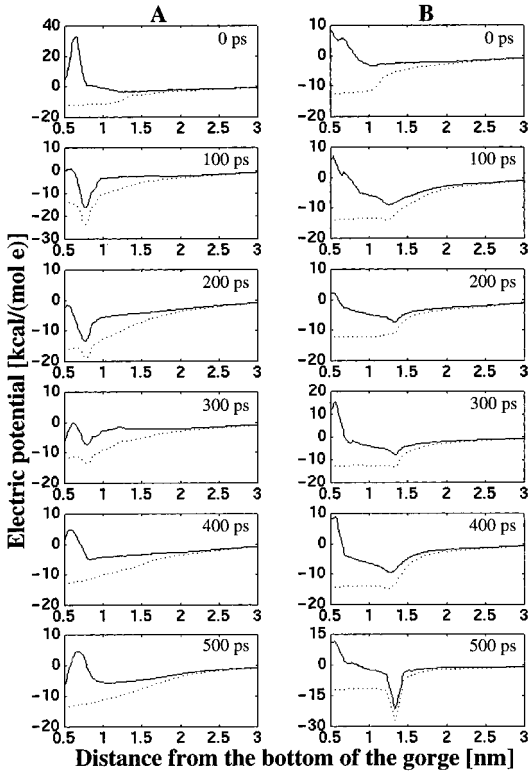

Figure 14. Variation of the electrostatic potential along the gorge axes (defined as in the caption of Figure 7), for selected snapshots of the AChE−THA complex. Dotted lines show the potential in the absence of the THA inhibitor, otherwise located between 0.5 and 1 nm above the gorge bottom. description.

play a role in AChE catalysis by providing ways for solvent transport into and out of the the enzyme active site.

Electrostatic Potential Fluctuation. Variations of the electrostatic potential along the reaction gorge for selected snapshots of AChE−THA and unliganded AChE (with the THA inhibitor removed) are shown in Figure 14. It is seen that the presence of a positively charged inhibitor not only increases the average electric potential but also decreases the positive part of its gradient inside the gorge (the entry to the gorge is approximately located at 2 nm from its bottom), which should slow the diffusion of the charged substrate toward the enzyme active site. In subunit B a potential minimum at about 1.3 nm has developed just after 100 ps. Closer examination of the gorge conformation reveals that the minimum is due to hydroxyl groups of Tyr 334 and Tyr 121 (residues which belong to a group of 14 aromatic residues lining the walls of the gorge) and one acidic residue (Glu 72) hydrogen bonded to Tyr 334. It is conceivable that such fluctuations in the potential might help to offset the steric bottleneck for binding cationic ligands in this region.[15]

Discussion

In this study we have used MD simulation of the entire TcAChE dimer to gain some insight into the function of this important enzyme. Although it is clear from the results presented that at 500 ps the enzyme continues to explore new parts of the phase space, its dynamic properties begin to converge after about 300 ps. We can expect therefore that the simulated motion samples the real dynamic behavior of the protein. Simulated atomic fluctuations derived from the last 100 ps show good agreement with the values obtained from X-ray experiments.

One of the motivations to simulate the entire AChE dimer was the possibility of the intermonomer contribution to the overall motion. We observed that indeed this kind of motion does occur, and it is visible starting from about 150−200 ps (Figure 3, 7, and 8). Its nature is a slight approach of the centers of mass ("cm's") of the subunits and simultaneous relative twisting of the subunits around a line passing through both monomers. This is a correlated motion contributing mostly to the first dominant mode, responsible for about 66.5% of the overall motion of the C_α atoms, and having 0.135 nm rms fluctuation from the cumulative average structure. It is difficult to say at this moment if this motion is of biological significance, although the displacements of the entrances to the gorges, the fluctuations of the electrostatic steering fields, and possible displacements of groups within the channels or active sites as components of this motion could all influence the activity of AChE.

TcAChE belongs to a lipase/esterase family sharing a structurally conserved element, a $L_{b3,2}$ cysteine loop.[42] In lipases the conformational flexibility of this element leads to a hinge-type motion which constitutes an essential mechanism for enzyme activation and substrate binding.[37−39] A similar mechanism has been recently proposed for AchE,[35,36] where the corresponding loop is a part of a thin portion of the gorge wall. The current room temperature simulation did not generate any extensive motion of the (Cys 67-Cys 94) loop similar to that observed in the MD simulation of human AChE after heating the enzyme to 1000 K.[36] Although we cannot conclude that such motion could not occur at a much longer simulation time, it may be that AChE does not use the lid-opening mechanism for substrate binding. On the other hand, our simulation shows that the (Cys 67-Cys 94) wall is like "Swiss cheese", having a capacity to form different openings alternative to the main channel. Small molecular species such as solvent molecules which participate in catalysis at the deacylation step, and small cations which might be needed to initiate catalysis[16] might therefore be able to pass through that wall. Although our simulation shows that the fluctuations of the primary reaction channel are fast and large enough so that the average closure of the channel is unlikely to seriously slow the catalysis, the permeability of the gorge wall for small molecules could add to the enzyme's efficiency. It is interesting that Axelsen et al. have observed previously the penetration of an NH_4^+ cation from the active site to the solvent in their MD simulation of the reaction gorge area of AChE,[43] while in the current simulation we observed bulk water molecules entering one of the numerous fluctuating side channels.

The electrostatic potential inside the reaction gorge provides a driving force for the charged ligand or substrate in the diffusional process of its binding by the enzyme active site,[14,15] In the current simulation we observed the fluctuation of that potential induced by protein motion, indicating that its gradient varies from strongly to less attractive for a positively charged ligand toward the bottom of the gorge. It is possible that while the instantaneous large attractive potential accelerates the complex formation, the less attractive phase will help the release of a positively charged product like choline, unless it penetrates through the gorge wall as suggested above. Cationic inhibitors like THA may rely in part on modifications of the potential to reduce the number of reactive encounters with the charged substrate (Figure 14).

(42) Cygler, M.; Schrag, J. D.; Sussman, J. L.; Harel, M.; Silman, I.; Gentry, M. K.; Doctor, B. P. *Protein Sci.* **1993**, *2*, 366−382.
(43) Axelsen, P. H.; Harel, M.; Silman, I.; Sussman, J. L. *Protein Sci.* **1994**, *3*, 188−197.

Table 2. Simulated and Experimental rms Fluctuations, and $rmsd_{X-ray}$ Values Averaged Over Secondary Structure Elements in Both Subunits of the AChE−THA Complex (in nm)[a]

			A		B	
helix/strand	residues	$\langle \Delta \mathbf{r}^2 \rangle^{1/2}_{exper}$	$\langle \Delta \mathbf{r}^2 \rangle^{1/2}_{sim}$	$rmsd_{X-ray}$	$\langle \Delta r^2 \rangle^{1/2}_{sim}$	$rmsd_{X-ray}$
h1	79−85	0.08	0.10	0.24	0.07	0.17
h2	132−139	0.09	0.07	0.10	0.08	0.14
h3	168−183	0.07	0.07	0.11	0.07	0.13
h4	200−211	0.06	0.05	0.08	0.05	0.07
h5	238−252	0.10	0.10	0.29	0.09	0.18
h6	259−268	0.11	0.11	0.37	0.11	0.25
h7	271−278	0.08	0.10	0.21	0.09	0.27
h8	305−311	0.09	0.09	0.29	0.09	0.16
h9	329−335	0.05	0.07	0.13	0.08	0.19
h10	349−360	0.09	0.10	0.20	0.10	0.21
h11	365−376	0.09	0.09	0.21	0.08	0.21
h12	384−411	0.07	0.07	0.14	0.07	0.14
h13	443−448	0.06	0.06	0.18	0.05	0.15
h14	460−479	0.09	0.08	0.16	0.08	0.15
h15	518−534	0.09	0.10	0.33	0.08	0.24
s1	6−10	0.11	0.09	0.16	0.09	0.18
s2	13−16	0.12	0.09	0.14	0.09	0.17
s3	18−21	0.11	0.09	0.29	0.09	0.17
s4	26−34	0.09	0.07	0.12	0.07	0.12
s5	57−60	0.11	0.09	0.16	0.08	0.20
s6	96−102	0.08	0.06	0.07	0.06	0.10
s7	142−147	0.08	0.05	0.09	0.05	0.10
s8	109−116	0.07	0.05	0.08	0.06	0.08
s9	193−199	0.08	0.05	0.15	0.05	0.14
s10	220−226	0.07	0.05	0.11	0.05	0.11
s11	318−334	0.07	0.06	0.14	0.06	0.17
s12	417−423	0.09	0.07	0.15	0.07	0.14
s13	502−505	0.09	0.08	0.16	0.07	0.12
s14	510−514	0.12	0.11	0.19	0.11	0.16
Cys^{67}-Cys^{94}	67−94	0.08	0.09	0.19	0.09	0.18

[a] Last row refers to the Cys^{67}-Cys^{97} loop.

Finally, we should mention that although similarities in the motion of the subunits are visible for the most mobile fragments of the proteins (Figures 4−6a), the subunits displayed asymmetrical behavior during the available time range of simulation. This asymmetry is visible in the somewhat different properties derived from the trajectory: the $rmsd_{X-ray}$ data for subunits (Figure 2, Tables 1 and 2), the structural differences between subunits in the cumulative average structure of the dimer (Figure 6), the distribution of the gorge sizes (Figure 10), the nature of the principal modes of motion, the frequency of side channel openings (Figure 12), and the shape of the electrostatic potential along the gorges (Figure 14). Obviously the simulation was too short to display the statistical equivalence of the subunits. The current simulation was done entirely using the EULER-GROMOS code run exclusively on the massively parallel Intel Paragon machine, using at least 128 processors and up to 256 processors (the maximum available to us for production simulation). Current parallel supercomputers are several times faster than this machine, so our simulation could now be done in a much shorter time. This holds the prospect of doing much longer simulations of AChE in the near future.

Conclusions

Our 0.5 ns MD simulation of AChE−THA dimer allows for the following conclusions:

1. The pattern of the atomic fluctuations of AChE−THA in solution is in reasonable qualitative agreement with the experimentally derived fluctuations from crystallography.

2. A large scale motion of slight contraction and relative rotation of the protein subunits has been detected. This motion belongs to the first dominant mode and consists mainly of a slight approach of the monomers toward each other and a small torsional motion of the two subunits relative to each other.

3. The fluctuations of the primary gorge opening have been characterized. The maximum opening seems to correspond roughly to the size of the substrate ACh, suggesting that the structure of the gorge and the electrostatic potential distribution within it are elements of AChE specificity.

4. Frequent formation of alternative entrances in the gorge wall have been observed, which may play a role in catalysis by providing an alternative way for molecular transport into and out of the enzyme active site.

5. The presence of the THA inhibitor in the active site of AChE not only prevents the proper alignment of the substrate but also decreases the gradient of the electrostatic potential in a way that would hinder substrate entry into the gorge.

Acknowledgment. We acknowledge generous support from the National Science Foundation, award number ASC-9217374 (which includes funds from DARPA). J.A.M. acknowledges support at UCSD from NSF, NIH, and the MetaCenters program of the NSF supercomputer centers.

JA971226D